

# Procedure for removing flow backgrounds from the charge-separation observable perpendicular to the reaction plane in heavy-ion collisions

Fufang Wen,<sup>1</sup> Liwen Wen,<sup>1</sup> and Gang Wang<sup>1</sup>

<sup>1</sup>*Department of Physics and Astronomy, University of California, Los Angeles, California 90095, USA*

Recent charge-dependent azimuthal correlation measurements in high-energy heavy-ion collisions have observed charge-separation signals perpendicular to the reaction plane, and the observations have been related to the chiral magnetic effect (CME). However, the correlation signal is contaminated with the background contributions due to the collective motion (flow) of the collision system, and it remains elusive to effectively remove the background from the correlation. We present a method study with Monte Carlo simulations and a multi-phase transport model, and develop a scheme to reveal the true CME signal via the event-shape engineering with the flow vector,  $\vec{q}$ . An alternative approach using the ensemble averages of observables is also discussed.

PACS numbers: 25.75.Ld

## I. INTRODUCTION

The thermodynamic states of the hot, dense, and deconfined nuclear medium created in high-energy heavy-ion collisions can be specified by the axial chemical potential  $\mu_5$ , as well as the temperature  $T$  and the vector chemical potential  $\mu$ . The quantity  $\mu_5$  characterizes the imbalance of right-handed and left-handed fermions in a system, and a *chiral* system bears a nonzero  $\mu_5$ . Chiral domains may be created locally in heavy-ion collisions through a variety of mechanisms on an event-by-event basis (e.g. topological fluctuations in the gluonic sector, glasma flux tubes, or fluctuations in the quark sector) [1–6]. In a noncentral collision, a strong magnetic field ( $B \sim 10^{15}$  T) can be produced (mostly by energetic spectator protons) [2, 3], and will induce an electric current along  $\vec{B}$  in chiral domains,  $\vec{J}_e \propto \mu_5 \vec{B}$ , which is called the chiral magnetic effect (CME) [1, 2]. On average,  $\vec{B}$  is perpendicular to the so-called reaction plane ( $\Psi_{RP}$ ) that contains the impact parameter and the beam momenta, as depicted in Fig. 1. Hence the CME will manifest a charge transport across the reaction plane.

In the presence of the CME and other modes of collective motions, we can Fourier decompose the azimuthal distribution of particles of given transverse momentum ( $p_T$ ) and rapidity:

$$\begin{aligned} \frac{dN_\alpha}{d\phi} &\propto 1 + 2v_{1,\alpha} \cos(\Delta\phi) + 2v_{2,\alpha} \cos(2\Delta\phi) + \dots \\ &+ 2a_{1,\alpha} \sin(\Delta\phi), \end{aligned} \quad (1)$$

where  $\phi$  is the azimuthal angle of a particle, and  $\Delta\phi = \phi - \Psi_{RP}$ . Here the subscript  $\alpha$  (+ or -) denotes the charge sign of the particle. Conventionally  $v_1$  is called “directed flow” and  $v_2$  “elliptic flow” [7]. The parameter  $a_1$  (with  $a_{1,-} = -a_{1,+}$ ) quantifies the charge separation due to the CME. However, from event to event, the signs of the  $\mu_5$  values are equally likely, and the signs of finite  $a_{1,+}$  and  $a_{1,-}$  will flip accordingly, leading to  $\langle a_{1,+} \rangle = \langle a_{1,-} \rangle = 0$ . One therefore has to search for the CME with charge-separation *fluctuations* perpendicular

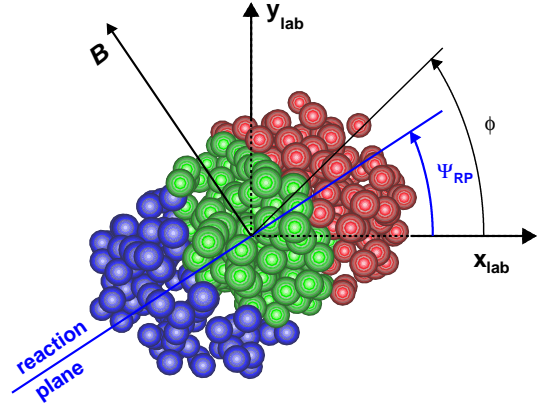


FIG. 1: (Color online) Schematic depiction of the transverse plane for a collision of two heavy ions (the left one emerging from and the right one going into the page). Particles are produced in the overlap region (green-colored nucleons). The azimuthal angles of the reaction plane and a produced particle used in the three-point correlator,  $\gamma$ , are depicted here.

to the reaction plane, e.g., with a three-point correlator [8],  $\gamma \equiv \langle \langle \cos(\phi_\alpha + \phi_\beta - 2\Psi_{RP}) \rangle \rangle_P \rangle_E$ , where the averaging is done over all particles in an event and over all events. In practice, the reaction plane is approximated with the “event plane” ( $\Psi_{EP}$ ) reconstructed with measured particles, and then the measurement is corrected for the finite event plane resolution.

The expansion of the  $\gamma$  correlator,

$$\begin{aligned} &\langle \langle \cos(\phi_\alpha + \phi_\beta - 2\Psi_{RP}) \rangle \rangle \\ &= \langle \langle \cos(\Delta\phi_\alpha) \cos(\Delta\phi_\beta) - \sin(\Delta\phi_\alpha) \sin(\Delta\phi_\beta) \rangle \rangle \\ &= [\langle v_{1,\alpha} v_{1,\beta} \rangle + B_{IN}] - [\langle a_{1,\alpha} a_{1,\beta} \rangle + B_{OUT}], \end{aligned} \quad (2)$$

reveals the difference between the *in-plane* and *out-of-plane* projections of the correlations. The first term ( $\langle v_{1,\alpha} v_{1,\beta} \rangle$ ) in the expansion provides a baseline unrelated to the magnetic field. The background contribution ( $B_{IN} - B_{OUT}$ ) is suppressed to a level close to the magnitude of  $v_2$  [8]. Previous

measurements from STAR and ALICE Collaborations reported a robust charge-separation signal from the opposite- and same-charge  $\gamma$  correlators ( $\gamma_{OS} > \gamma_{SS}$ ) in Cu+Cu/Au+Au/Pb+Pb/U+U collisions with the center-of-mass energy from 19.6 GeV to 2.76 TeV [9–14]; see Ref. [15] for a recent review of the experimental results. However, the apparent charge separation is still contaminated with the  $v_2$ -related background. For example, owing to elliptic flow, there are more clusters flying in-plane than out-of-plane, which is irrelevant to the CME, but the decays of the clusters (into particles with opposite charges) will contribute to the charge separation across the reaction plane. Similar effects also hold when elliptic flow is coupled with transverse momentum conservation (TMC) and/or local charge conservation (LCC) [16–18].

Flow backgrounds could be potentially removed via the so-called event-shape engineering (ESE) [19, 20], with which *spherical* events or sub-events are selected, so that the particles of interest therein carry zero  $v_2$ . A previous attempt was made with a charge-separation observable roughly equivalent to  $\gamma$ , as a function of event-by-event “observed  $v_2$ ” [21]. However, there are several issues in this approach that prevent a clear interpretation of the result. In Sec II, we offer a few caveats in the practice of the ESE, and develop an effective scheme to restore the CME signal with Monte Carlo simulations and a hybrid transport model (AMPT) [22, 23]. We further discuss a substitute approach with ensemble averages of observables in Sec III.

## II. EVENT-SHAPE ENGINEERING

A valid ESE approach requires three key components. First, a good handle on the event shape is needed to truly reflect the ellipticity of each event or sub-event. This requirement may seem obvious and easy to satisfy, but as will be demonstrated later even with a simple Monte Carlo simulation, it is not as trivial as it sounds. Second, the finite flow background has to vanish when the event-shape handle is turned to the zero-flow position. Here the AMPT model that contains only backgrounds but no signals, will serve the illustration purpose. Third, the event selection by turning a proper handle should not create an artificial background, or if it does, the impact has to be under control. To study this effect, we will again use the simulation that contains only signals but no backgrounds.

### A. Handle on event shape

In the flow analysis, it is a common practice to divide each event into two sub-events, A and B, and reconstruct the event plane  $\Psi_{EP}^B$  with particles in B, and then corre-

late particles in A with  $\Psi_{EP}^B$  [7]:

$$v_2^{\text{observe}} \equiv \langle \cos[2(\phi^A - \Psi_{EP}^B)] \rangle_P. \quad (3)$$

$\Psi_{EP}^B$  is the azimuthal angle of the reconstructed flow vector,  $\vec{q}^B = (q_x^B, q_y^B)$ :

$$q_x^B = \frac{1}{\sqrt{N}} \sum_i^N \cos(2\phi_i^B) \quad (4)$$

$$q_y^B = \frac{1}{\sqrt{N}} \sum_i^N \sin(2\phi_i^B). \quad (5)$$

Here for simplicity, we ignore the weights that are often assigned to the particles for the event plane reconstruction in practice. The true  $v_2$  of particles in A (with respect to the true reaction plane) will be measured by

$$v_2^A = v_2^{\text{observe}} / R^B, \quad (6)$$

where  $R^B \equiv \langle \cos[2(\Psi_{EP}^B - \Psi_{RP})] \rangle_E$  is the event plane resolution of  $\Psi_{EP}^B$  [7]. The single-bracket means the averaging over events. The sub-event-plane method described above has been extensively used and proven by many to be valid on ensemble average.

In the ESE approach, it is tempting to introduce an event-by-event “ $v_2$ ” observable,

$$v_{2,\text{ebye}}^{\text{observe}} \equiv \langle \cos[2(\phi^A - \Psi_{EP}^B)] \rangle_P, \quad (7)$$

and to select “spherical” sub-events with the condition that  $v_{2,\text{ebye}}^{\text{observe}} = 0$ , as was implemented in Ref. [21]. However, zero  $v_{2,\text{ebye}}^{\text{observe}}$  does not necessarily mean that particles in A have zero  $v_2^A$ .

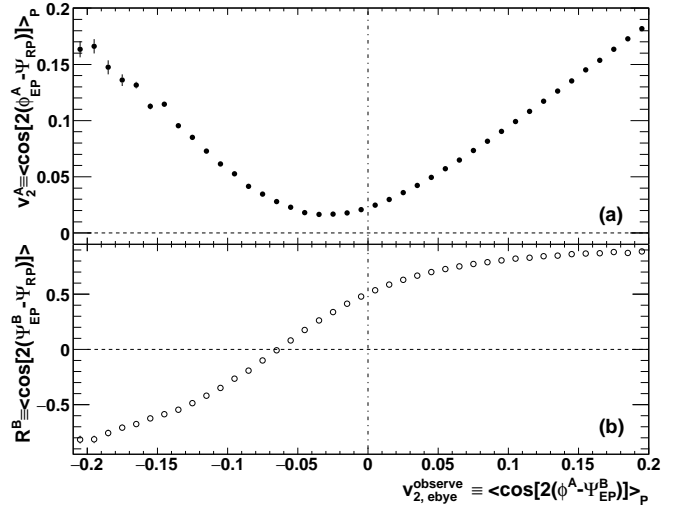


FIG. 2: The true elliptic flow  $v_2^A$  (upper) and the true event plane resolution  $R^B$  (lower) as functions of  $v_{2,\text{ebye}}^{\text{observe}}$ , from Monte Carlo simulations.

The relationship between  $v_2^A$  and  $v_{2,\text{ebye}}^{\text{observe}}$  has been investigated in a Monte Carlo simulation. In each event,

the azimuthal angle of each particle has been assigned randomly according to the distribution of Eq. (1). In this Monte Carlo simulation, only  $v_2$  and  $a_1$  are nonzero, and non-flow effects such as TMC, LCC and resonance decay have not been implemented. In other words, there are only elliptic flow and the charge separation due to the CME, but no background contributions. We have fixed the input parameters with realistic values so that  $v_2 = 5\%$  and  $|a_{1,\pm}| = 2\%$ . Each of the 10 million simulated events contains 400 charged particles, with 200 positively charged and 200 negatively charged.

The upper panel of Fig. 2 presents the simulation results of  $v_2^A$  as a function of  $v_{2,\text{ebye}}^{\text{observe}}$ , which interestingly displays a U-shape, with the minimum above zero. This means that truly spherical sub-events can never be selected however the  $v_{2,\text{ebye}}^{\text{observe}}$  handle is turned. Or at least, the sphericity of a sub-event (A) depends on the choice of the *beholder* ( $\Psi_{\text{RP}}$  or  $\Psi_{\text{EP}}^{\text{B}}$ ), if the event-by-event “ $v_2$ ” observable is the selection criterion. Worse still is the fact exhibited in the lower panel that  $R^{\text{B}}$ , the true event plane resolution of  $\Psi_{\text{EP}}^{\text{B}}$ , strongly depends on  $v_{2,\text{ebye}}^{\text{observe}}$ , and could become negative. This makes it highly non-trivial to correct for the event plane resolution, when the same  $\Psi_{\text{EP}}^{\text{B}}$  is used to calculate  $v_2^A$  or  $\gamma^A$  differentially as a function of  $v_{2,\text{ebye}}^{\text{observe}}$ . In practice, the negative  $R^{\text{B}}$  values are hardly obtainable. The more disturbing caveat comes from the combined information from both panels:

$$v_2^A \neq v_{2,\text{ebye}}^{\text{observe}} / R^{\text{B}}, \quad (8)$$

with the  $v_{2,\text{ebye}}^{\text{observe}}$ -binning scheme. Therefore, even with the knowledge of  $R^{\text{B}}$ , it is unlikely to restore the value of an observable with respect to the true reaction plane in a  $v_{2,\text{ebye}}^{\text{observe}}$  bin. Eqs. (6) and (8) tells that the underlying factorization assumption for the correction for the event plane resolution holds on ensemble average and breaks down on the  $v_{2,\text{ebye}}^{\text{observe}}$  basis.

A good handle on event shape should reflect the sphericity property of the sub-event of interest, which is independent of the beholder. One candidate is  $q$ , the magnitude of the flow vector reconstructed with particles in the sub-event A (with the same procedure as  $\vec{q}^{\text{B}}$  in Eqs. (4) and (5)). By definition,  $q$  has no explicit contributions from the sub-event B or the reaction plane. In reality, there could be implicit correlations between  $q$  and  $\Psi_{\text{EP}}^{\text{B}}$  due to flow fluctuations, which will be discussed in Sec II B. Figure 3(b) presents the Monte Carlo simulation results of the true elliptic flow  $v_2^A$  and the corrected observable  $v_2^{\text{observe}}$  as functions of  $q$ . On the  $q$  basis, the correction for the event plane resolution is valid, and both  $v_2$  values approach zero at vanishing  $q$ . Note that the success in a simple simulation does not guarantee the success in real-data analyses, which can be complicated by various realistic factors, but if an approach (like the  $v_{2,\text{ebye}}^{\text{observe}}$  basis) fails even in a simple simulation, it should be definitely be avoided in data analyses.

$q$  turns out to be a good handle on event shape, but not as good as  $q^2$ .  $q^2 = 0$  implies  $q = 0$ , so  $q^2$  naturally inherits the capability of selecting spherical events

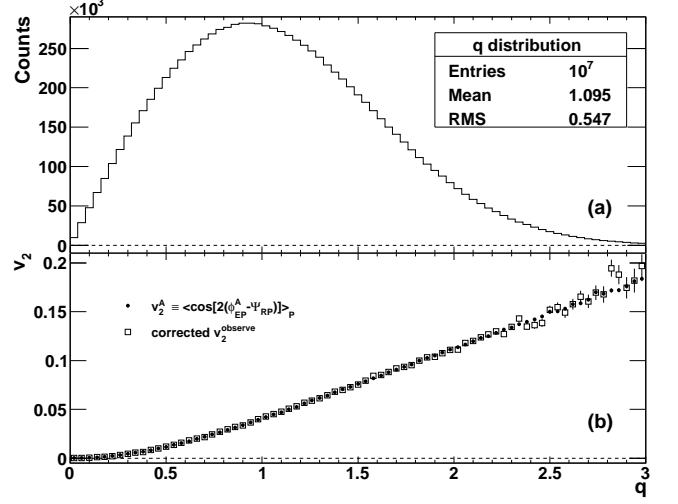


FIG. 3: The distribution of  $q$  (upper), and the true elliptic flow  $v_2^A$  and the corrected  $v_2^{\text{observe}}$  as functions of  $q$  (lower), from Monte Carlo simulations.

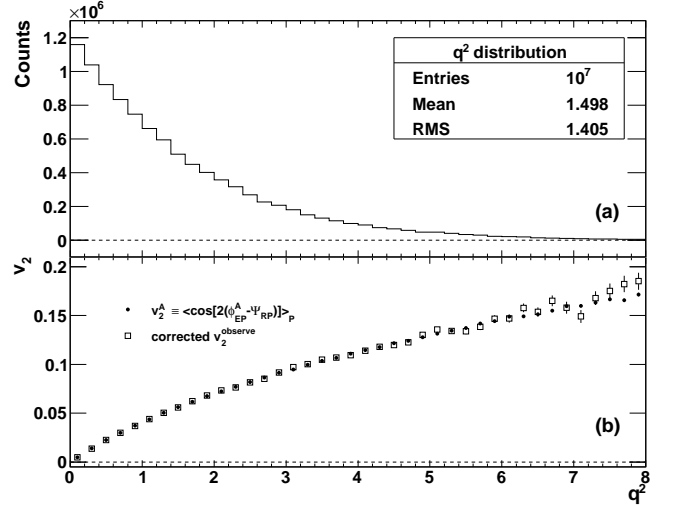


FIG. 4: The distribution of  $q^2$  (upper), and the true elliptic flow  $v_2^A$  and the corrected  $v_2^{\text{observe}}$  as functions of  $q^2$  (lower), from Monte Carlo simulations.

in the second harmonic. Moreover, Fig. 4(b) displays an almost linear relationship between  $v_2^A$  ( $v_2^{\text{observe}}$ ) and  $q^2$  at low  $q^2$ , which conveniently enables the linear projection of  $\gamma_A$  to  $q^2 = 0$ , to remove  $v_2$ -related backgrounds. Another advantage of  $q^2$  over  $q$  lies in their distributions, shown in Fig. 3(a) and Fig. 4(a). The  $q$  distribution peaks around unity, and rapidly drops on both sides. This feature means lower statistics towards lower  $q$ , so the projection of an event-by-event observable to  $q = 0$  becomes unstable. On the other hand, the  $q^2$  distribution is “squeezed” in phase space towards zero, technically facilitating a robust projection to zero  $q^2$ .

### B. Disappearance of background

The AMPT model [22, 23] is a realistic event generator that has been widely used to describe experimental data. The string melting version of AMPT [23, 24] reasonably well reproduces particle spectra and elliptic flow in Au+Au collisions at 200 GeV and Pb+Pb collisions at 2.76 TeV [25]. The CME is not included in AMPT, which simplifies the background study.  $5.5 \times 10^6$  AMPT events are generated for 200 GeV Au+Au collisions. Each event has been divided into three sub-events according to pseudorapidity,  $\eta$ : sub-event A contains particles of interest with  $|\eta| < 1.5$ , and sub-event B1(B2) serves as a sub-event plane using particles with  $1.5 < \eta < 4$  ( $-4 < \eta < -1.5$ ).  $\Psi_{EP}^{B1}$  and  $\Psi_{EP}^{B2}$  are separately used to calculate  $v_2$  or  $\gamma$ , and the two sets of results are combined to achieve better statistics. The corresponding sub-event plane resolution is obtained via correlation:  $R^B \equiv \sqrt{\langle \cos[2(\Psi_{EP}^{B1} - \Psi_{EP}^{B2})] \rangle}$ .

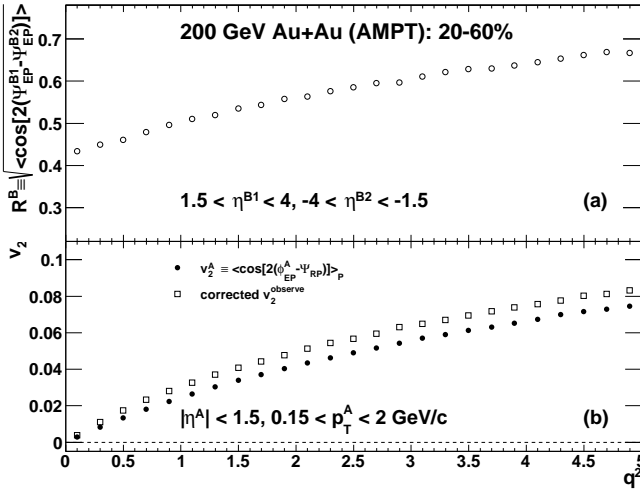


FIG. 5: The sub-event plane resolution (upper), and the true elliptic flow  $v_2^A$  and the corrected  $v_2^{\text{observe}}$  as functions of  $q^2$  (lower), from AMPT simulations.

Figure 5 shows the sub-event plane resolution (upper), and the true elliptic flow  $v_2^A$  and the corrected  $v_2^{\text{observe}}$  as functions of  $q^2$  (lower), from AMPT simulations of 20 – 60% Au+Au collisions at  $\sqrt{s_{NN}} = 200$  GeV. Unlike the simple Monte Carlo simulation in which  $R^B$  is constant over  $q^2$ , AMPT events involve flow fluctuation that causes a positive correlation in flow between sub-events in the same event, and as a result,  $R^B$  increases with  $q^2$ . The lower panel displays a discrepancy between  $v_2^A$  and the corrected  $v_2^{\text{observe}}$ , which is not a sign of the breakdown of the underlying factorization assumption (as in Eq. 8), but due to the difference between the reaction plane and the participant plane [26], in terms of non-flow and flow fluctuation. What matters more is the fact that both  $v_2$  values decreases with  $q^2$ , and drop to (0, 0).

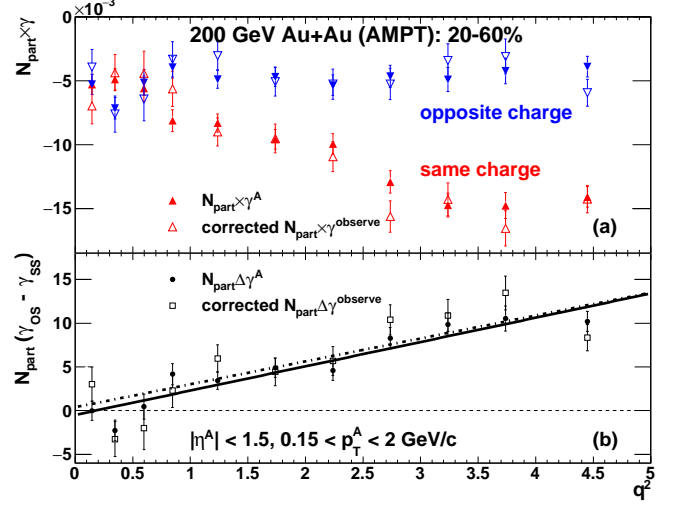


FIG. 6: (Color online)  $N_{\text{part}} \times \gamma$  (upper) and  $N_{\text{part}} \Delta\gamma$  (lower) as functions of  $q^2$ , from AMPT simulations. The full (open) symbols represent results obtained with the true reaction plane (reconstructed event plane, with correction for the event plane resolution). The solid (dashed) line in the lower panel is a linear fit of the full (open) data points.

In the upper panel of Fig. 6, we present the  $\gamma$  correlators multiplied by the number of participating nucleons,  $N_{\text{part}}$ , as functions of  $q^2$ , for 20 – 60% AMPT events of Au+Au collisions at 200 GeV. Here  $N_{\text{part}}$  is used to compensate for the dilution effect due to the later-stage rescattering [27]. For both the same-charge and the opposite-charge correlators, the true  $\gamma^A$  and the corrected  $\gamma^{\text{observe}}$  are consistent with each other within the statistical uncertainties. This indicates that compared with  $v_2$ ,  $\gamma$  is less sensitive to non-flow or flow fluctuation. At larger  $q^2$ , the opposite-charge correlators are above the same-charge correlators, suggesting a finite flow-related background. The opposite- and same-charge correlators converge at small  $q^2$ . The lower panel shows  $N_{\text{part}} \Delta\gamma \equiv N_{\text{part}}(\gamma_{\text{OS}} - \gamma_{\text{SS}})$  vs  $q^2$ , and again, the two observables seem to coincide. Linear fits to both observables yield small intercepts that are consistent with zero:  $(-4.9 \pm 6.1) \times 10^{-4}$  for  $N_{\text{part}} \Delta\gamma^A$  and  $(3.9 \pm 9.9) \times 10^{-4}$  for  $N_{\text{part}} \Delta\gamma^{\text{observe}}$ . The finite  $\Delta\gamma$  values in AMPT events are solely due to background contributions, so the disappearance of background is demonstrated when the “correctable” observable ( $\Delta\gamma$ ) is projected to zero  $q^2$ . Here the linear fits only serve for illustration purposes, and the optimal projection scheme is subject to the details of the measured  $\Delta\gamma(q^2)$ .

### C. Artificial signal/background

To study the relationship between two observables, special attention has to be paid to the intrinsic correlation between their definitions. For example, when  $\gamma_{\text{ebye}}$



is plotted against  $v_{2,\text{ebye}}$  (both are obtained with the true reaction plane), a finite slope often exists even if there is no explicit physical correlation between the two. This can be understood by expanding  $\gamma_{\text{ebye}}$ :

$$\begin{aligned}\gamma_{\text{ebye}} &\equiv \langle \cos(\phi_\alpha + \phi_\beta - 2\Psi_{\text{RP}}) \rangle_{\text{P}} \\ &= \langle \cos[(\phi_\alpha - \phi_\beta) + 2(\phi_\beta - \Psi_{\text{RP}})] \rangle_{\text{P}} \\ &= \langle \cos(\phi_\alpha - \phi_\beta) \cos[2(\phi_\beta - \Psi_{\text{RP}})] \rangle_{\text{P}} \\ &\quad - \langle \sin(\phi_\alpha - \phi_\beta) \sin[2(\phi_\beta - \Psi_{\text{RP}})] \rangle_{\text{P}} \\ &\approx 2\delta_{\text{ebye}}v_{2,\text{ebye}} + C,\end{aligned}\quad (9)$$

where  $C$  is a constant, and  $\delta_{\text{ebye}} \equiv \langle \cos(\phi_\alpha - \phi_\beta) \rangle_{\text{P}}$ , is the two-particle correlation, that contains various contributions such as  $a_{1,\alpha}a_{1,\beta}$ , resonance decay, TMC, LCC, etc.  $\delta$  is usually finite, leading to a finite apparent slope in  $\gamma_{\text{ebye}}$  vs  $v_{2,\text{ebye}}$ , which could be misinterpreted as physics signal/background. The coefficient “2” in front of  $\delta_{\text{ebye}}v_{2,\text{ebye}}$  is the sum of 1.5 contributed by the  $\langle \cos(\dots)\cos(\dots) \rangle$  term and 0.5 by the  $-\langle \sin(\dots)\sin(\dots) \rangle$  term. Without loss of generality, we apply the initial condition that on ensemble average  $\gamma_{\alpha\beta}$  is  $-a_{1,\alpha}a_{1,\beta}$ , and then the constant  $C$  (or intercept) becomes  $-a_{1,\alpha}a_{1,\beta} - 2\delta v_2$ .

As discussed in Sec. II B, the flow background disappears when  $q^2 = 0$ , therefore any finite  $\Delta\gamma$  signal at zero  $q^2$  in experimental measurements will evidence a charge separation truly due to the CME. However, a finite signal at zero  $q^2$  is not necessarily equal to the ensemble-averaged signal. Fig. 7 illustrates the artificial effect with the simple Monte Carlo simulation, where  $|a_1|$  and  $v_2$  are fixed at 2% and 5%, respectively, and there is no input of any background or any explicit correlation between  $|a_1|$  and  $v_2$ . The apparent slope in  $\gamma_{\text{SS}}$  ( $\gamma_{\text{OS}}$ ) vs  $q^2$  follows the sign of  $\delta_{\text{SS}}$  ( $\delta_{\text{OS}}$ ), which results from Eq. 9 because  $q^2$  is almost linearly related to  $v_2$  at small  $q^2$  (see Fig. 4(b)). Note that the disappearance of background validates  $\delta_{\text{SS}} = -\gamma_{\text{SS}}$  and  $\delta_{\text{OS}} = -\gamma_{\text{OS}}$ . Although the ensemble average of  $\gamma_{\text{SS}}$  ( $\gamma_{\text{OS}}$ ) is  $-4 \times 10^{-4}$  ( $4 \times 10^{-4}$ ), the apparent value at zero  $q^2$  exaggerates the charge separation by relative  $2v_2$  (10% in this case).

Figure 8 sketches our proposal to experimentally reveal the true CME signal via the ESE. First, the proper handle on event shape,  $q^2$ , is employed. Second, the flow background is removed by projecting the charge-separation observable to zero  $q^2$ . Third, the ensemble-averaged CME signal is restored from  $\Delta\gamma(q^2 = 0)/(1 + 2v_2)$ . This scheme is not unique to the  $\gamma$  correlator, and could be applied to other similar observables, such as the modulated sign correlator (MSC) [11] and the charge multiplicity asymmetry correlator (CMAC) [21].

### III. ENSEMBLE AVERAGE

The ESE with  $q$ , when applicable, provides an effective solution to remove flow backgrounds. However, in case of  $\gamma$  correlations with identified particles, especially rare particles,  $q$  could become statistically unstable with the

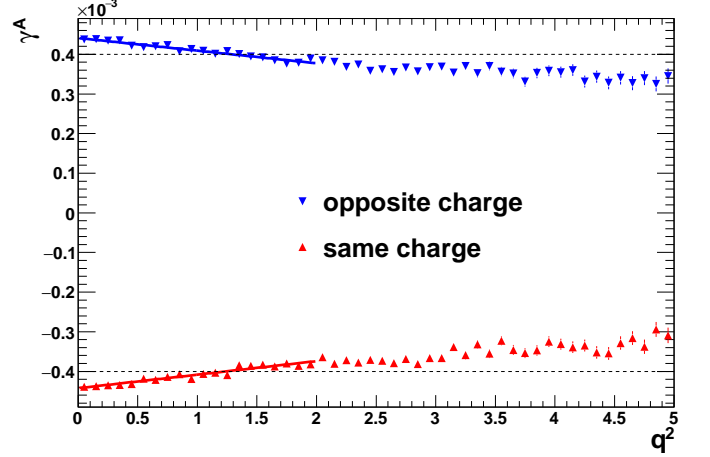


FIG. 7: (Color online)  $\gamma$  obtained with the true reaction plane as a function of  $q^2$ , from the Monte Carlo simulation. The solid lines are linear fits of the points.

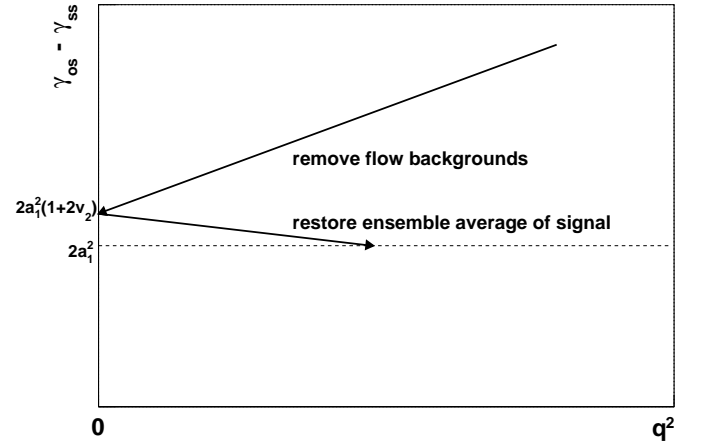


FIG. 8: A schematic diagram of how to reveal the ensemble-averaged CME signal via the ESE.

number of particles under study as low as two per event. In this situation, we resort to the ensemble averages of several observables to subtract flow backgrounds.

The  $\gamma$  correlator by construction contains the background terms  $B_{\text{IN}}$  and  $B_{\text{OUT}}$ , and their difference was originally studied for the “flowing cluster” case [8]:

$$\frac{B_{\text{IN}} - B_{\text{OUT}}}{B_{\text{IN}} + B_{\text{OUT}}} \approx v_{2,\text{cl}} \frac{\langle \cos(\phi_\alpha + \phi_\beta - 2\phi_{\text{cl}}) \rangle}{\langle \phi_\alpha - \phi_\beta \rangle}, \quad (10)$$

where  $\phi_{\text{cl}}$  is the cluster emission azimuthal angle, and  $\phi_\alpha$  and  $\phi_\beta$  are the azimuthal angles of two decay products. The flowing cluster can be generalized to a larger portion of or even the whole event, through the mechanisms of TMC and/or LCC. For example, the TMC effect leads to the following pertinent correlation terms in  $\delta$  and  $\gamma$  [17]:

$$\delta \rightarrow -\frac{1}{N} \frac{\langle p_T \rangle_\Omega^2}{\langle p_T^2 \rangle_F} \frac{1 + (\bar{v}_{2,\Omega})^2 - 2\bar{v}_{2,F}\bar{v}_{2,\Omega}}{1 - (\bar{v}_{2,F})^2}, \quad (11)$$

$$\gamma \rightarrow -\frac{1}{N} \frac{\langle p_T \rangle_\Omega^2}{\langle p_T^2 \rangle_F} \frac{2\bar{v}_{2,\Omega} - \bar{v}_{2,F} - \bar{v}_{2,F}(\bar{v}_{2,\Omega})^2}{1 - (\bar{v}_{2,F})^2} \approx \kappa \cdot v_{2,\Omega} \cdot \delta, \quad (12)$$

where  $\kappa = (2\bar{v}_{2,\Omega} - \bar{v}_{2,F})/v_{2,\Omega}$ , and  $\bar{v}_2$  and  $\bar{v}_2$  represent the  $p_T$ - and  $p_T^2$ -weighted moments of  $v_2$ , respectively. The subscript “F” denotes an average of all produced particles in the full phase space; the actual measurements will be only in a fraction of the full space, denoted by “ $\Omega$ ”. The background contribution due to the LCC effect has a similar characteristic structure as the above [16, 18].

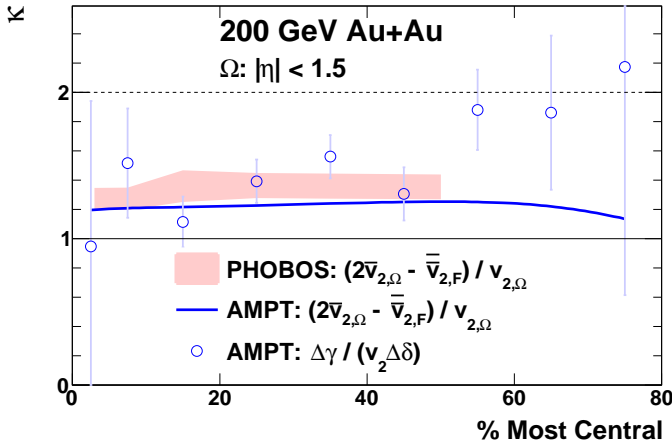


FIG. 9: Estimation of  $\kappa$  with three approaches for 200 GeV Au+Au.

It is convenient to express  $\gamma$  and  $\delta$  with a two-component framework [12, 17]:

$$\gamma \equiv \langle \cos(\phi_\alpha + \phi_\beta - 2\Psi_{RP}) \rangle = \kappa v_2 B - H, \quad (13)$$

$$\delta \equiv \langle \cos(\phi_\alpha - \phi_\beta) \rangle = B + H, \quad (14)$$

where  $H$  and  $B$  are the CME and background contributions, respectively. The background-subtracted correlator,  $H$ , can be obtained from the ensemble averages of several observables:

$$H^\kappa = (\kappa v_2 \delta - \gamma)/(1 + \kappa v_2). \quad (15)$$

The major uncertainty in the above expression, the coefficient  $\kappa$ , depends on particle charge combination and particle transverse momentum. It may also depend on centrality and collision energy, reflecting slightly different particle production mechanism in different conditions.

Figure 9 shows the  $\kappa$  values estimated for Au+Au collisions at 200 GeV, with the  $v_2$  measurements by the PHOBOS collaboration [28, 29], and with the  $v_2$  calculations from the AMPT model. Here only the TMC effect has been taken in account, and  $\kappa$  is typically within [1.2, 1.4] for  $|\eta| < 1.5$ . The  $\kappa$  values attained this way will vary slightly if a smaller  $|\eta|$  acceptance is involved. In reality,  $\kappa$  should be averaged over various mechanisms such as TMC, LCC and resonance decays. The AMPT model gives a more comprehensive estimate in Fig. 9 via

$\Delta\gamma/(v_2\Delta\delta)$ , where the numerator is solely due to flow backgrounds. For the centrality range of 10–50%, where the statistical uncertainties are small, the  $\kappa$  values thus obtained are close to those estimated with the  $v_2$  information.

It is not the aim of this article to precisely determine  $\kappa$  via  $\Delta\gamma/(v_2\Delta\delta)$  from AMPT, which is statistically demanding. Instead, we want to illustrate the feasibility of this approach, and further call for a data-driven exercise to extract  $\kappa$ . For the  $\gamma$  correlations with all charged particles, the ESE with  $q$  is applicable, so the true CME signal (and hence the true background) can be measured. The true background,  $(\Delta\gamma - \Delta H)$ , divided by the measured  $v_2(\Delta\delta - \Delta H)$ , will yield the realistic  $\kappa$  value (most of the time,  $\Delta H \ll \Delta\delta$ ). Then with the assumption that  $\kappa$  is roughly universal for different particles, the CME signal can be revealed on ensemble average even in the  $\gamma$  measurements with rare particles. Another worthwhile practice is to express the observed charge separation in the “ $\kappa$ ” unit by defining  $\kappa^{\text{CME killer}} \equiv \Delta\gamma/(v_2\Delta\delta)$ , which is the  $\kappa$  value needed to force  $\Delta H$  to be zero. Accordingly, if a measured  $\kappa^{\text{CME killer}}$  is significantly above two (the upper bound of all estimated  $\kappa$  values), it evidences a real charge-separation signal due to the CME. On the other hand, if a  $\kappa^{\text{CME killer}}$  is close to one (the lower bound of  $\kappa$  values), it is unlikely to claim a CME signal.

#### IV. SUMMARY

The experimental searches for the CME in heavy-ion collisions have aroused extensive attention, and special efforts are required to disentangle the CME-induced charge-separation signal from the flow-related backgrounds. We have disclosed a few shortcomings of a previous attempt of the ESE with  $v_{2,\text{ebye}}^{\text{observe}}$  [21]. The root cause lies in the fact that  $v_{2,\text{ebye}}^{\text{observe}}$  is a correlation between two symmetric sub-events, instead of a property of any sub-event. Therefore, the selection of a given  $v_{2,\text{ebye}}^{\text{observe}}$  value triggers an event-shape bias in either sub-event, making neither suitable to serve as an unbiased event plane. For example,  $v_{2,\text{ebye}}^{\text{observe}} = 0$  implies that the two sub-event planes,  $\Psi_{EP}^A$  and  $\Psi_{EP}^B$ , are  $\pm 45^\circ$  from each other, and neither sub-event has to be spherical. In this case, when one sub-event (A) is beheld by the other (B), which is either  $45^\circ$  or  $-45^\circ$  away (not necessarily with equal possibility), the sense of being in-plane or out-of-plane is impaired, because the two possible scenarios of  $\Psi_{EP}^B$  are perpendicular to each other. As a result, the observed charge separation is artificially reduced at  $v_{2,\text{ebye}}^{\text{observe}} = 0$ .

The magnitude of the flow vector,  $q$ , or even better,  $q^2$ , emerges to be a good handle on event shape.  $q$  or  $q^2$  reflects the sphericity property of the sub-event of interest, and zero  $q$  selects spherical sub-events in the second harmonic.  $q^2$  is technically better than  $q$ , because  $q^2$  is almost proportional to  $v_2$  at low  $q^2$ , and the  $q^2$  distribution favors the projection of  $\gamma$  to zero  $q^2$ . The AMPT model has been exploited to verify the disappearance of

flow backgrounds at zero  $q^2$ , and simple Monte Carlo simulations have been utilized to study the artificial correlations in the ESE process. Based on these findings, we have designed an effective recipe to experimentally remove flow backgrounds and restore the ensemble average of the CME signal.

When the reconstruction of  $q$  is hindered by the low multiplicity of rare particles, an alternative path can be adopted with the ensemble averages of several observables to retrieve the CME signal. The background quantifier,  $\kappa$ , has been estimated in three approaches, and we

further propose the fourth, a data-driven practice. In the end, the “ $\kappa$ ” unit is advocated to investigate the competition between the CME signal and flow backgrounds.

**Acknowledgments:** We thank Huan Huang and other members of the UCLA Heavy Ion Physics Group for discussions, and we are grateful to Ning Yu for the help with AMPT. We also benefit from the fruitful discussions with Fuqiang Wang. This work is supported by a grant (No. DE-FG02-88ER40424) from U.S. Department of Energy, Office of Nuclear Physics.

- 
- [1] D. E. Kharzeev, L. D. McLerran and H. J. Warringa, Nucl. Phys. A **803**, 227 (2008)
  - [2] D. Kharzeev, Phys. Lett. B **633**, 260 (2006).
  - [3] D. Kharzeev and A. Zhitnitsky, Nucl. Phys. A **797**, 67 (2007).
  - [4] D. Kharzeev, A. Krasnitz and R. Venugopalan, Phys. Lett. B **545**, 298 (2002).
  - [5] I. Iatrakis, S. Lin and Y. Yin, Phys. Rev. Lett. **114**, 252301 (2015).
  - [6] K. Fukushima, D. E. Kharzeev and H. J. Warringa, Phys. Rev. Lett. **104**, 212001 (2010).
  - [7] A. M. Poskanzer and S. Voloshin, Phys. Rev. C **58**, 1671 (1998).
  - [8] S. A. Voloshin, Phys. Rev. C **70**, 057901 (2004).
  - [9] B. I. Abelev *et al.* [STAR Collaboration], Phys. Rev. Lett. **103**, 251601 (2009).
  - [10] B. I. Abelev *et al.* [STAR Collaboration], Phys. Rev. C **81**, 54908 (2010).
  - [11] L. Adamczyk *et al.* [STAR Collaboration], Phys. Rev. C **88**, 064911 (2013).
  - [12] L. Adamczyk *et al.* [STAR Collaboration], Phys. Rev. Lett. **113**, 052302 (2014).
  - [13] B. I. Abelev *et al.* [ALICE Collaboration], Phys. Rev. Lett. **110**, 021301 (2013).
  - [14] Gang Wang *et al.* [STAR Collaboration], Nucl. Phys. A **904-905**, 248c (2013).
  - [15] D.E. Kharzeev, J. Liao, S.A. Voloshin and G. Wang, Prog. Part. Nucl. Phys. **88**, 1 (2016).
  - [16] S. Pratt, S. Schlichting and S. Gavin, Phys. Rev. C **84**, 024909 (2011).
  - [17] A. Bzdak, V. Koch and J. Liao, Lect. Notes Phys. **871** 503 (2013) [arXiv:1207.7327 [nucl-th]].
  - [18] S. Schlichting and S. Pratt, Phys. Rev. C **83**, 014913 (2011).
  - [19] S. A. Voloshin, Phys. Rev. Lett. **105**, 172301 (2010).
  - [20] J. Schukraft, A. Timmins and S. A. Voloshin, Phys. Lett. B **719**, 394 (2013)
  - [21] L. Adamczyk *et al.* [STAR Collaboration], Phys. Rev. C **89**, 044908 (2014).
  - [22] B. Zhang, C.M. Ko, B.-A. Li and Z.-W. Lin, Phys. Rev. C **61**, 067901 (2000).
  - [23] Z.-W. Lin, C.M. Ko, B.-A. Li and B. Zhang, Phys. Rev. C **72**, 064901 (2005).
  - [24] Z.-W. Lin and C.M. Ko, Phys. Rev. C **65**, 034904 (2002).
  - [25] Z.-W. Lin, Phys. Rev. C **90**, 014904 (2014).
  - [26] J. -Y. Ollitrault, A. M. Poskanzer and S. A. Voloshin, Phys. Rev. C **80**, 014904 (2009).
  - [27] G. L. Ma and B. Zhang, Phys. Lett. B **700**, 39 (2011).
  - [28] B. alver *et al.* [PHOBOS Collaboration], Phys. Rev. C **83**, 024913 (2011).
  - [29] B.B Back *et al.* [PHOBOS Collaboration], Phys. Rev. C **72**, 051901(R) (2005).